ELSEVIER

Journal of Alloys and Compounds 460 (2008) 191–195

Journal of ALLOYS AND COMPOUNDS

www.elsevier.com/locate/jallcom

Synthesis and characterization of Ag doped Cu nanoparticles

C. Duhamel, J.L. Bonnentien, Y. Champion *

ICMPE-CNRS UMR 7182, Université Paris 12, 15, rue Georges Urbain, 94407 Vitry-sur-Seine Cedex, France

Received 1 December 2006; received in revised form 16 May 2007; accepted 17 May 2007
Available online 21 May 2007

Abstract

The synthesis of $Cu_{100-x}Ag_x$ ($0.05\,at.\% < x < 0.30\,at.\%$) nanoparticles using an evaporation–condensation process has been studied. Particular attention has been paid to the composition of the as-prepared powders. Compared to the master alloy, systematic enrichment in Ag of the particles is observed at the beginning of the synthesis but a continuous decrease in the Ag content of the powders is observed during the process. Even though, after de-agglomeration, the chemical composition of the powders is, in average, homogeneous. We have shown that optimized synthesis conditions give spherical particles with a mean diameter of 50 nm and a reasonable yield rate.

Keywords: Nanocrystalline particles; Copper; Condensation; X-ray diffraction

1. Introduction

Decreasing the grain size of a polycrystalline material leads to a higher volume fraction of the intercrystalline regions (grain boundaries and triple junctions) [1]. For small grain sizes, typically $d < 100$ nm, the intergranular zones become non-negligible (atomic fraction in grain boundaries, GB >1%) and are likely to influence the properties of the material, among which the mechanical behavior. It has been reported that, in ultrafine-grained metals, non-equilibrium GB and low angle GB lead to higher stress levels [2] whereas high angle GB favor dislocation absorption and grain recovery [3]. Ma et al. [4] have shown that nano-twinned copper, with a mean lamellae spacing of 200 nm exhibits significantly enhanced ductility under tensile loading. However, although extensive studies are carried out on this topic, the micro-mechanisms responsible for such a behavior are still unclear. An alternative approach to understand the role of GB is to compare nanocrystalline metals with various GB chemistries. This purpose needs to synthesize bulk nanocrystalline metals which GB are selectively doped with foreign atoms. It should be emphasized as well, that the presence of impurities at the GB should increase the stability of nanocrystalline materials by inhibiting both mechanically and thermally driven grain growth [5,6].

The powder metallurgy technique is one of the main routes to produce bulk nanocrystalline metals. Synthesis of fully dense bulk nanocrystalline copper by densification of nanoparticles has already been achieved [7]. The as-prepared material exhibits interesting mechanical properties such as a near-perfect elasto-plastic behavior with 12% ductility in tension [8]. The synthesis of the nanoparticles is the first step of the processing route. In an attempt to obtain bulk nanocrystalline metals with GB doped with foreign elements, the nanopowders have to fulfill several requirements: (i) a small particle size, (ii) a spherical shape to facilitate further densification, (iii) a reasonable yield rate and (iv) a good chemical homogeneity. The nanopowders are produced using the cryogenic melting technique. This technique is based on the evaporation of a molten metallic droplet immersed in a cryogenic liquid and the condensation of the surrounding supersaturated metallic vapor [9]. Production of nanoparticles of pure metals such as Cu, Fe and Al with a reasonable yield rate has been already successfully achieved [10,11]. However, gas condensation techniques are rarely used to synthesize nanoparticles of alloys [12–14]. Because of the difference in the evaporation rates of the two elements, deviation in composition between the master alloy and the resulting powders is expected and the final composition of the particles is usually unpredictable [15].

The present work reports on the synthesis and characterization of Ag doped Cu nanoparticles prepared by the cryogenic melting technique. The chemical composition and the homogeneity of the as-prepared powders have been carefully

* Corresponding author. Tel.: +33 56 70 30 41; fax: +33 1 46 75 04 33.
E-mail address: champion@glvt-cnrs.fr (Y. Champion).

0925-8388/$ – see front matter © 2007 Elsevier B.V. All rights reserved.
doi:10.1016/j.jallcom.2007.05.064

analyzed. The crystalline structure, the size and morphology of the powders have been investigated as well as the influence of the processing conditions on these parameters.

2. Choice and composition of the Ag doped Cu system

The main objective of this work is to synthesize nanoparticles in order to fabricate *in fine* a nanocrystalline material selectively doped at GB with foreign atoms. For this purpose, a relevant binary system has to be defined. Segregation of the solute element towards the GB is possible if it reduces the interfacial energy. The segregated atoms have thus to fulfill two criteria: (i) miscibility gap with the solvent atom, (ii) high segregation enthalpy. According to the equilibrium phase diagram [16], no solid solution of Ag in Cu can be formed at room temperature. The experimentally measured segregation enthalpy of Ag in Cu is $-40\,\mathrm{kJ\,mol^{-1}}$ [17,18]. Although it is lower than the one of Bi in Cu [19], Ag was selected because it does not modify drastically the mechanical properties of the materials. Especially, no embrittlement of Cu due to Ag segregation has been reported [20,21].

In order to avoid Ag precipitation, the atomic fraction required to saturate the GB, as the upper limit of Ag content, has to be determined. To estimate the grain size dependence of the Ag amount at GB saturation, the model of a regular fourteen-sided tetrakaidecahedron for the grains shape [22] was used. The total intercrystalline surface is:

$$S_{IC} = \frac{V_{IC}}{2\delta} = \frac{V_{total}}{2\delta}\left[1-\left(1-\frac{\delta}{d}\right)^3\right] \approx \frac{V_{total}}{2\delta} \times \left[1-\left(1-3\frac{\delta}{d}\right)\right] \approx \frac{3V_{total}}{2d} \quad (1)$$

V_{IC} is the intercrystalline volume, V_{total} the total volume, d the grain size and δ is the grain boundary thickness. At low Ag content:

$$V_{total} \approx \frac{m_{Cu}}{\rho_{Cu}} \approx \frac{NM_{Cu}}{\rho_{Cu}N_A} \quad (2)$$

m_{Cu} is the Cu weight, M_{Cu} the Cu molar weight, ρ_{Cu} the Cu density, N_{total} the total number of atoms and N_A is the Avogadro number.

Assuming that all the Ag atoms segregate at the grain boundaries and that all the segregation sites are equivalent, it comes:

$$\frac{N_{Ag}}{S_{IC}} = \frac{x_{Ag}N_{total}}{S_{IC}} = \frac{2x_{Ag}\rho_{Cu}N_A d}{3M_{Cu}} \quad (3)$$

where x_{Ag} is the atomic fraction of Ag and N_{Ag}/S_{IC} stands for the saturation solute excess in the GB. Theoretically, saturation of a GB by a solute atom is reached for one monolayer of the doping element. According to Hondros and Seah [23], one atomic monolayer contains $\Omega^{2/3}$ solute atoms per unit surface, where Ω is the atomic volume. For Ag, this leads to $N_{Ag}/S_{IC} = 12.6\,\mathrm{at./nm^2}$ and with the nanoparticles size equal to 50 nm, Eq. (3) gives $x_{Ag} = 0.45$ at.%. Experimental results show that saturation is generally reached before one complete monolayer is formed at the Cu GB [18]. Electron energy loss spectroscopy experiments [20] have revealed that only one upon four segregation sites is occupied, i.e. 0.26 monolayer and saturation should be expected for 0.11 at.%. The atomic fraction of 0.45 at.% is certainly an overestimate, though it gives the relevant range of compositions that can be prepared.

3. Experimental

Ingots of master alloys were prepared by melting commercial copper and silver (purity 99.99%) in levitation by radio frequency induction. The as-prepared ingots are then shaped by melting under a He atmosphere and cold rolled to obtain a 6 mm diameter rod. Nanoparticles are produced from the as-prepared rod using the cryogenic melting technique. A 30-g droplet of the master alloy is overheated and maintained in levitation in the evaporating device filled with liquid nitrogen. The droplet is regularly fed with the alloy bar in order to balance the weight loss of the droplet and to prevent from any change of its position in the evaporating device during the synthesis. During evaporation, a calefaction layer forms around the droplet in which nanoparticles are instantaneously condensed. They are conveyed, thanks to the nitrogen flow, towards linen filters where they are collected. In order to reveal deviation in the composition during the synthesis, nanoparticles are collected in a first filter during the first 15–30 min of evaporation and in second for the last 15–30 min. In the following, the two batches will be called "start" and "end", respectively. Since nanopowders are pyrophoric, they are stored in hexane where they are slowly oxidized by reaction with dilute O_2 and H_2O.

The average compositions of the master-alloys and the nanopowders were measured by inductively coupled plasma/optical emission spectroscopy (ICP/OES). The morphology and the size distribution of the particles were controlled by observations using transmission electron microscopy (TEM, JEOL 2000EX microscope operating at 200 kV). X-ray diffraction (XRD) patterns were performed using a Philips generator operating at 40 kV and 30 mA with Co Kα radiation ($\lambda_{\alpha1} = 1.78896$ Å and $\lambda_{\alpha2} = 1.79285$ Å). Treatment of the patterns was carried out with the EVA software (Brüker). In particular, the mean particles size was estimated from the X-ray line profile analysis [24] using the modified Halder–Wagner plot, proposed by Ungar et al. [25], which takes into account the stacking faults and/or twins density:

$$\left(\frac{\beta^* - TW}{d^*}\right)^2 = \frac{\beta^* - TW}{\varepsilon d^{*2}} + \eta^2 \quad (4)$$

where β^* is the modified integral breadth $\beta^* = \beta\cos\theta/\lambda$, T the adjustable parameter depending on the planar faults density, W the Warren-Averbach anisotropy constants, η the internal strain and ε is the coherently diffracting domain size. The mean particles diameter D is given by $D = 4/3\varepsilon$, where 4/3 is a correcting factor taking into account the spherical shape of the particles.

4. Results and discussion

The nanopowders were prepared from three different master alloys with Ag content of 0.05, 0.15 and 0.30 at.%. At 2000 K, which corresponds to the temperature range reached during the synthesis, the vapor pressure is of 50 Torr for Ag and 5 Torr for Cu [26], respectively. Accordingly, Ag should evaporate faster than Cu and the resulting powders should be enriched in Ag. However, a previous study on the synthesis of Fe–Ni nanopowders using the same technique has shown that the alloys usually do not react as an ideal mixture. The preferential evaporation of either one or the other constituent depends on the composition range [15] and the relation between the composition of the master alloy and that of the resulting powders is then unpredictable.

The compositions of the as-prepared powders corresponding to each master alloy are reported in Table 1. A large scattering between the composition of the powders "start" and the pow-

Table 1
Silver content in at.% of the master ingot and the "start" and "end" powders obtained from the corresponding master alloy

Batch	Master ingot (%)	Powders "start" (%)	Powders "end" (%)
1	0.277 ± 0.007	0.750 ± 0.006 0.700 ± 0.006 0.690 ± 0.011	0.295 ± 0.007 0.268 ± 0.007
2	0.135 ± 0.005	0.201 ± 0.011	0.120 ± 0.002
3	0.135 ± 0.005	0.198 ± 0.011	0.134 ± 0.002
4	0.051 ± 0.003	0.053 ± 0.002	0.028 ± 0.002
5	0.051 ± 0.003	0.095 ± 0.003 0.068 ± 0.002	0.045 ± 0.002 0.016 ± 0.002

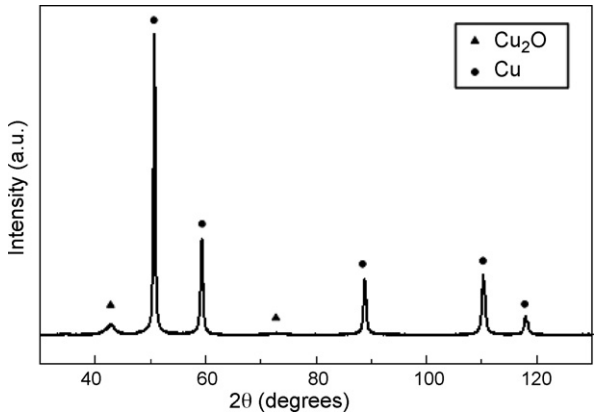

Fig. 1. X-ray diffraction pattern of nanopowders containing 0.045 at.% Ag and produced with an apparent power of 46 kW.

ders "end" is observed. The powders collected at the beginning of the synthesis are largely enriched in Ag compared to the initial rod. The Ag content can reach twice that of the master alloy. In contrast, the powders collected at the end of the process have generally a lower Ag content than the initial rod. These results show that, for the used synthesis conditions and for this range of composition, Ag evaporates preferentially to Cu. At the beginning of the process, the composition of the molten droplet of master alloy is Cu_xAg_{1-x}. The powders obtained after a time δt have an average composition Cu_yAg_{1-y} with $y < x$. During the same time δt, the silver content in the droplet of master alloy also decreases. In order to compensate the loss of mass and to adjust the composition, the molten droplet is fed with the master alloy rod. However, this is not sufficient to maintain the initial composition of the droplet and the composition becomes $Cu_{x'}Ag_{1-x'}$ with $x' > x$. As described previously, after a time δt, this droplet will lead to the formation of powders with an average composition of $Cu_{y'}Ag_{1-y'}$ with $y' < x'$ but also $y' < y$ as a lower Ag content in the metal droplet will necessary lead to a lower Ag content in the powders. This process goes on all along the synthesis and explains the deviation of composition both between the powders and the master alloy but also, for a same master alloy, between the powders produced at the beginning and at the end of the synthesis.

According to this process, each batch is composed of particles with different compositions and, thus, should be chemically heterogeneous. The average composition of different samples taken from the same batch has been checked before (batches 1 and 5) and after (batch 3) de-agglomeration of the powders (Table 1). For batches 1 and 5, a substantial scattering (from 9 to 180%) in the compositions is observed. In the contrary, the compositions of nine samples taken from batch 3 "start" are quite similar as they range between 0.198 and 0.204 at.%. Even though deviation of composition occurs during the synthesis of the powders, after de-agglomeration, a batch of these powders is macroscopically chemically homogeneous. De-agglomeration of the powders induces a relevant mixing and is thus particularly important.

The synthesis of nanoparticles is the first step of a global process leading to the production of fully densified bulk nanocrystalline alloys [14]. For this reason, the size and the shape of the as-prepared powders are particularly important. The smallest the particles are, the smallest grain size is likely to be obtained in the bulk sample. Further densification of the powders is partially done by cold compaction, which is optimized when the particles are perfectly spherical in shape. At last, the yield of the process should be high enough to enable the production of the 10 g of powders necessary to produce one bulk sample. The only parameter easily adjustable to optimize the synthesis of nanoparticles using the cryogenic melting technique is the apparent power P_{app} supplied by the high frequency generator to the inductor. One part of the apparent power is used to melt the alloy whereas the other part maintains the metallic droplet in

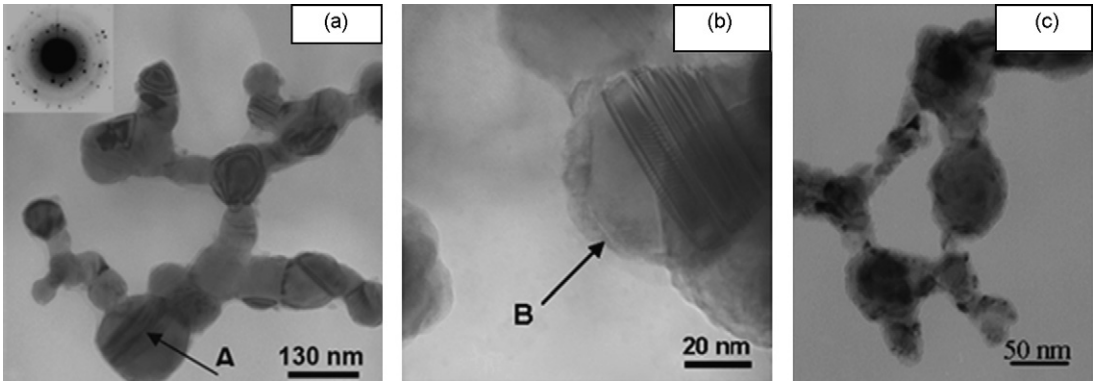

Fig. 2. TEM micrograph of Cu–Ag nanoparticles after synthesis with an apparent power of (a) and (b) 46 kW; (c) 61 kW. The inset in (a) shows the corresponding selected-area electron diffraction pattern. Twins are observed in some of the particles (arrow A). The particles are covered by an oxide layer (arrow B).

levitation in the inductor. The higher the power is, the higher the levitation force is and the higher the droplet is in the inductor. In the contrary, when the power is too low, levitation is no more possible.

Nanopowders have been synthesized using three different apparent powers: 46, 50 and 61 kW. For $P_{app} = 46$ kW, the X-ray diffraction pattern of powders containing 0.045 at.% Ag is shown in Fig. 1. Two phases are co-existing: a Cu-rich phase and the oxide Cu_2O which comes from the soft oxidation in hexane. No peak characteristic of an Ag-rich phase is detected. The volume fraction of the oxide is estimated around 25 vol.% from the X-ray lines (this value is confirmed by the TEM observations showing an average 2.5 nm thick layer of oxide surrounding the particles). The lattice parameter measured is equal to 0.3616 ± 0.0001 nm and is similar to the one obtained for nanoparticles of pure copper. According to the TEM micrographs (Fig. 2a and b), some of the particles contain twins (arrow A) coming from the synthesis process. Except for the oxide layer, no contrast due to chemical heterogeneities is detected and the electronic diffraction pattern exhibits the characteristic rings of the fcc structure of a Cu-rich phase as well as two rings characteristic of Cu_2O. Similar features are obtained for all the other synthesized particles, independently of the chemical composition and the applied power. Both X-ray diffraction analyses and TEM observations suggest that Ag forms a supersaturated solid solution with Cu in the nanoparticles. According to the equilibrium phase diagram, no solid solution of Ag in Cu can exist at room temperature [16]. However, numerous metastable supersaturated Cu-rich and Ag-rich solid solutions, have been obtained in the Cu–Ag system by vapor quenching or liquid quenching [16]. During the synthesis, the Cu–Ag alloy is in non-equilibrium conditions, which is likely to lead to a metastable Cu-rich solid solution. Similar enhanced solubility limits have already reported in nanoparticles for different binary systems such as Fe–Ni, Ag–Fe, Ti–Mg or Cu–Bi [1,15].

The size and the shape of the particles as well as the yield rate for each apparent power are reported in Table 2. The particles size, estimated from the X-ray diffraction patterns, is measured from the slope of the modified Halder–Wagner plot Fig. 3a.

Table 2
Particles size, particles shape and yield rate for different apparent powers supplied to the inductor during the synthesis of the powders

Apparent power (kW)	Particles size (nm)	Particles shape	Yield rate (g min^{-1})
61	63	Not well-defined	0.52
50	51	Spherical	0.605
46	47	Spherical	0.62

When the apparent power decreases from 61 to 46 kW, the average particles size decreases from 63 to 47 nm. The values obtained from the XRD analysis are in agreement with the mean grain estimated from TEM micrographs by manual counting over around 200 particles. As shown in Fig. 3b the particles size distribution has a log-normal shape, characteristic for nanoparticles prepared by gas condensation techniques [27]. For the powders with 0.045 at.% Ag prepared at 46 kW, the particles size ranges between 20 and 170 nm with an average value equal to 52 nm. The TEM micrographs shown in Fig. 2 reveal that for the lowest power, the particles are spherical and only agglomerated by weak bonding, such as Van der Waals forces (Fig. 2a and b). When the power increases, the particles do not have a well-defined shape and are very agglomerated with sintering necks between some of them (Fig. 2c). At last, an increase of the yield rate from 0.52 to 0.62 g min^{-1} is observed with a decrease in the apparent power from 61 to 46 kW (Table 2). To summarize, the lowest apparent power (46 kW) supplied to the inductor leads to the finest, less agglomerated and more spherical particles and to the highest yield. Such a trend has already been reported for nanoparticles of pure copper [28].

In order to correlate the size and the shape of the particles and the yield rate to the apparent power, it is important to understand the phenomena occurring, during the synthesis, in the calefaction layer between the molten metallic droplet and the cryogenic liquid. In the calefaction layer, the formation of the particles follows three different steps: nucleation, growth and agglomeration. During the nucleation step, the critical size and the number of stable nuclei depend on the supersaturation ratio S defined by

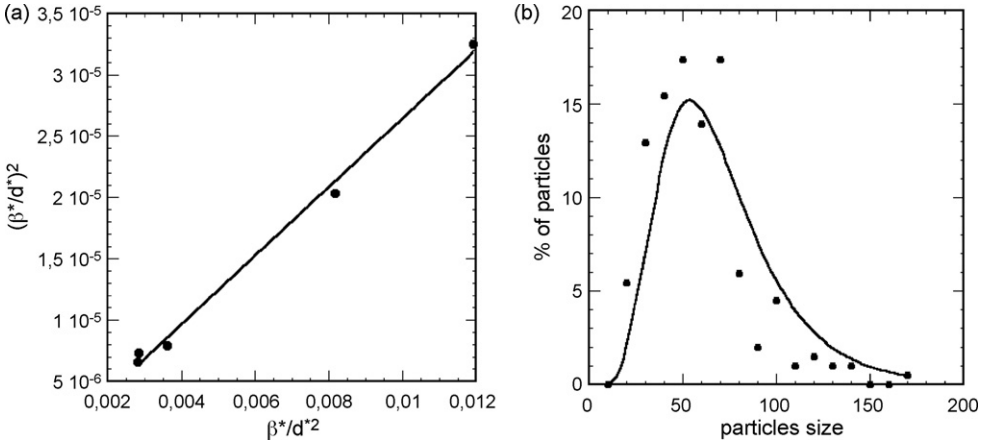

Fig. 3. (a) Modified Halder–Wagner analysis and (b) particles size distribution for nanopowders containing 0.045 at.% Ag and produced with an apparent power of 46 kW. The dots refer to the experimental data obtained from TEM micrographs by manual counting over 200 particles. The solid line is a log-normal distribution calculated from the experimental data.

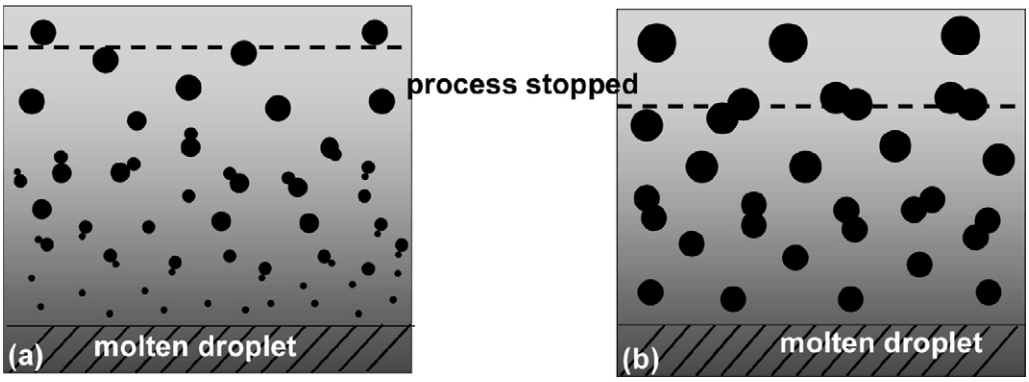

Fig. 4. Schematic illustration of the phenomena occurring in the calefaction layer during the synthesis for (a) $P_{app} = 46$ kW; (b) $P_{app} = 61$ kW. The dashed line represents the end of the process.

$$S = \frac{P}{P_0} \tag{5}$$

where P is the pressure close to the molten metallic droplet and P_0 is the vapor saturating pressure. According to the homogeneous nucleation model, the critical nucleus size is inversely proportional to ln(S) whereas the number of stable nuclei is directly proportional to S. A higher S value leads to a larger quantity of smaller particles. The major drawback is that a high supersaturation rate also enhances the coalescence and growth of the formed stable nuclei, leading to a substantial increase in the particles size. Experimentally, the supersaturation rate can be modified by changing the temperature of the molten droplet, i.e. by changing the apparent power supplied to the inductor. Fig. 4 is a schematic description of the phenomena suspected in the calefaction layer for apparent powers of 46–61 kW. When the apparent power is low, the droplet is in the lower part of the inductor and the temperature supplied to the liquid metal is high. A high number of very fine stable nuclei are formed but, because of the high supersaturation rate, they grow and coalesce quickly. The well-defined spherical shape of the particles for the lower power suggests that the synthesis process is stopped by the cryogenic liquid just after a coalescence step, as shown in Fig. 4. In the contrary, for a high apparent power, the molten droplet is in the upper part of the inductor and the temperature is lower. Fewer nuclei with a larger critical size are formed, which results in a lower yield. Fewer coalescence events occur but this is not sufficient to counterbalance the difference in the nuclei critical size between the low and high power. Therefore, in spite of a longer time in the calefaction layer, the finest particles are obtained for $P_{app} = 46$ kW. The agglomeration and bonding observed for $P_{app} = 61$ kW suggest that the process is stopped in the middle of a coalescence step.

5. Summary

Synthesis and characterization of Ag doped Cu nanoparticles prepared by the cryogenic melting technique have been reported. Because of the differences in the vapor pressure of the two metals, deviation in composition between the master alloy and the powders occurs. At the beginning of the synthesis, the powders are systematically enriched with Ag but the silver content continuously decreases during the process. We have shown that a relevant de-agglomeration of the powders leads to a macroscopically homogeneous chemical composition. Optimized synthesis conditions give spherical particles with a mean diameter of 50 nm. The crystalline structure consists in a metastable supersaturated solid solution of Ag in Cu.

References

[1] C. Suryanarayana, Int. Mater. Rev. 40 (1995) 41.
[2] N. Krasilnikov, M.W. Lojkowski, Z. Pakiela, R.Z. Valiev, Mater. Sci. Eng. A 397 (2005) 330.
[3] P.L. Sun, C.Y. Yu, P.W. Kao, C.P. Chang, Scripta Mater. 52 (2004) 265.
[4] E. Ma, Y.M. Wang, Q.H. Lu, M.L. Sui, L. Lu, K. Lu, Appl. Phys. Lett. 85 (2004) 4932.
[5] J.M.C. Li, Phys. Rev. Lett. 96 (2006) 215506.
[6] J. Weismüller, Nanostruct. Mater. 3 (1993) 261.
[7] C. Langlois, M.J. Hytch, P. Langlois, S. Lartigue-Korinek, Y. Champion, Metall. Mater. Trans. A 36 (2005) 3451.
[8] Y. Champion, C. Langlois, S. Guérin-Mailly, P. Langlois, J.-L. Bonnetien, M.J. Hytch, Science 300 (2003) 310.
[9] Y. Champion, Ann. Chim. Sci. Mater. 31 (2006) 281–294.
[10] Y. Champion, J. Bigot, Scripta Mater. 35 (1996) 517.
[11] Y. Champion, J. Bigot, Nanostruct. Mater. 10 (1998) 1097.
[12] T. Haubold, Acta Metall. Mater. 41 (1993) 1769.
[13] H. Konrad, et al., Nanostruct. Mater. 7 (1996) 605.
[14] M.N.A. Karlsson, K. Deppert, L.S. Karlson, M.H. Magnuson, Aerosol Sci. Tech. 38 (2004) 948.
[15] C. Duhamel, Y. Champion, M. Walls, M. Tencé, J. All. Comp. 393 (2005) 204.
[16] P.R. Subramanian, J.H. Perepezko, J. Phase Equilib. 14 (1993) 62.
[17] J. Bernardini, Z. Tökei, D.L. Beke, Phil. Mag. A 73 (1996) 237.
[18] S. Divinski, M. Lohmann, C. Herzig, Acta Mater. 49 (2001) 29.
[19] S. Divinski, M. Lohmann, C. Herzig, Acta Mater. 52 (2004) 3973.
[20] J. Bruley, V.J. Keast, D.B. Williams, Acta Mater. 47 (1999) 4009.
[21] R. Schweinfest, A.T. Paxton, M.W. Finnis, Nature 432 (2004) 1008.
[22] G. Palumbo, S.J. Thorpe, K.T. Aust, Scripta Met. Mater. 24 (1990) 1347.
[23] E.D. Hondros, M.P. Seah, Int. Met. Rev. 222 (1977) 262.
[24] J.E. Langford, Accuracy in Powder Diffraction II, 846, National Institute of Standards and Technology, Gaithersburg, MD, USA, 1992, p. 145 (Special Publication).
[25] T. Ungár, S. Ott, P.G. Sanders, A. Borbély, J.R. Weertman, Acta Mater. 46 (1998) 3693.
[26] R.E. Honig, RCA Rev. 23 (1962) 567.
[27] C.G. Granqvist, R.A. Buhrman, J. Appl. Phys. 47 (1976) 2200.
[28] Y. Champion, J.L. Bonnentien, C. Langlois, C. Duhamel, J. Moulin, F. Mazaleyrat, P. Bayle, M.J. Hÿtch, Mater. Sci. For. 436–442 (2003) 2411.